ATLAS Internal Note
INDET-NO-202
5 March 1998

Thermal simulation of ATLAS barrel SCT modules - II

T. Kondo, T. Haruyama, T. Kohriki, H. Iwasaki, S. Terada, Y. Unno

KEK, High Energy Accelerator Organization
Institute of Particle and Nuclear Study
1-1, Oho, Tsukuba-shi, 305, Japan

July 27, 1997

Abstract

A finite element thermal analysis is performed for the ATLAS barrel SCT module. The design of the module are based on the TDR model. Its several variations are also evaluated. The goal of the present calculation is to estimate the safety margin for the thermal runaway and its dependence on various design parameters.

1. Module design

As a follow-up of the previous thermal simulation study on various module designs [1], two module geometries and their variations are evaluated as listed in Table 1. Model TDR-1 is the geometry proposed in the ATLAS ID TDR [2]. Model TDR-2 is a model with no BeO stiffeners (see pictures). Figure 1 shows the models TDR-1 and TDR-2. The 40 mrad tilting of stereo angle is neglected for simplicity.

Table 1 Module models

model	variation	description
TDR-1	1	TDR model
	1a	right PG replaced by BeO
	1b	all BeO baseboard
	1c	BeO attachment at the cooling side
	1d	shorter PG nose by 1cm
	1e	longer PG nose by 1cm
	1f	all PG baseboard
	1g	all PG baseboard, no stiffener at cooling side
	1h	all PG baseboard, CFRP inserts
	1i	model-1h but insulator on the non-cooling side
TDR-2	2	No stiffeners, BeO frame
	2a	no BeO bypass in the middle
	2b	inclined PG nose

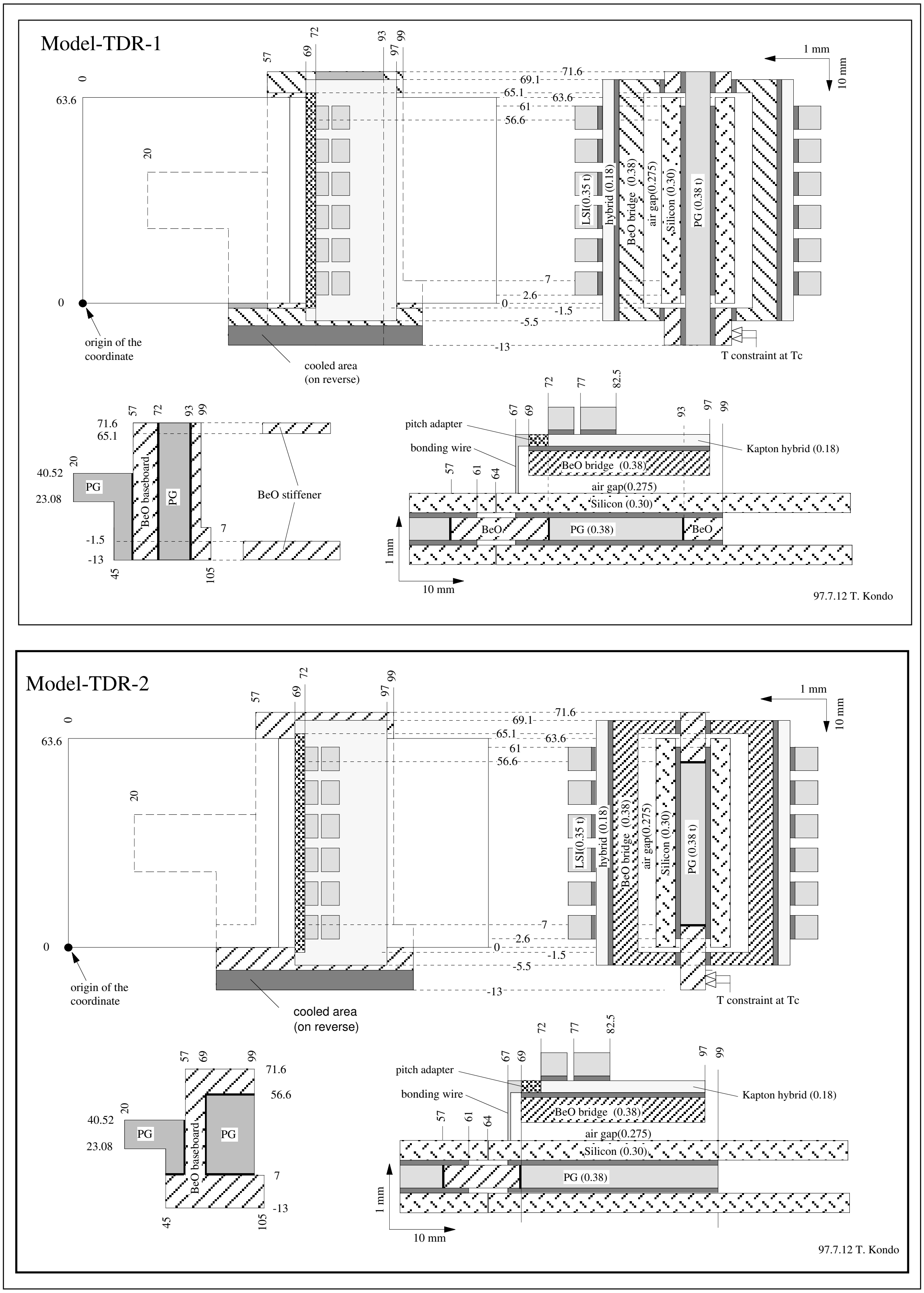

Figure 1 Model TDR-1(with stiffeners) and TDR-2 (without stiffeners).

Present study is to find optimum geometry of the baseboard, the essential component of the heat transfer. Figure 2 shows the various configuration of the baseplate under study.

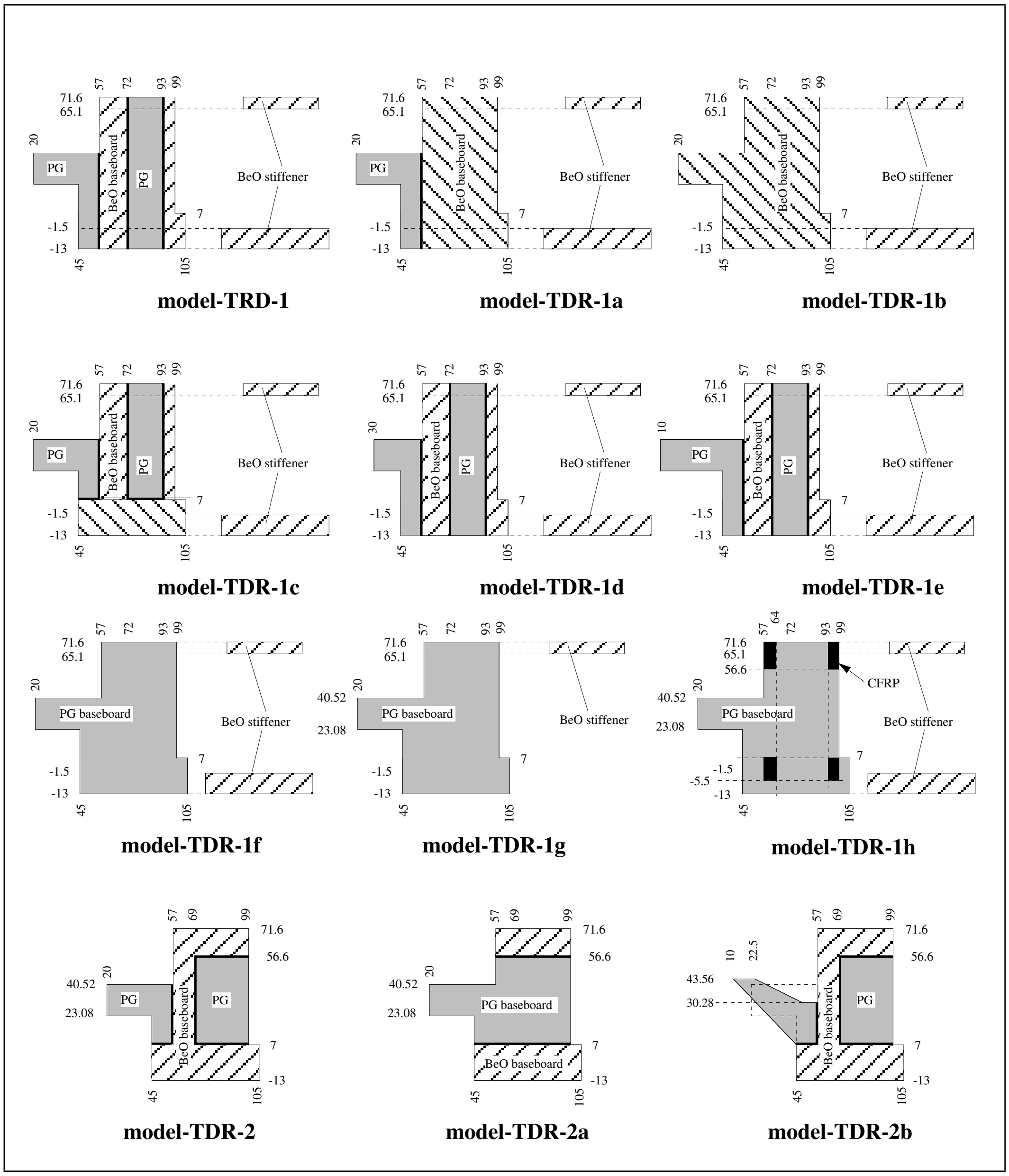

Figure 2 Design of the baseboard.

2. Thermal simulation

2.1 Material constants:

A finite-element thermal simulation is done using program ANSYS 5.1. A 3-D thermal and electrical solid elements is used. The thermal conductivity used in the program is listed in Table 2.

It is noted that a gluing gap of 0.1 mm in width is introduced at the boundaries between

Table 2 Thermal conductivity of material used in the ANSYS simulation

material	conductivity (W/m·K)	material	conductivity (W/m·K)
silicon	130	BeO	280
PG700	700 (tangential) 3.5 (normal)	PG1300	1300 (tangential) 3.5 (normal)
PG1700	1700 (tangential) 3.5 (normal)	CFRP	25 (tangential) 1 (normal)
thermal glue	0.5	Kapton hybrid	0.25
air	0.0245	BeO hybrid	280
quartz (fan-in)	0.15	bonding wire	150

the BeO and PG baseboards since its effect in non-negligible. In addition air is introduced between the BeO bridge and silicon detector surface. Bonding wires between the pitch adapter and silicon detector, though their effects turned out to be thermally negligible,

2.2 Constraints and environments:

For simplicity, the effects of surface convection and radiation emission are not included.

The cooling pipe is not included in the simulation. Instead, the temperature constraint is imposed at the contact of the cooling channel. The open triangle marks in the design figures show the location of this external constraint.

2.3 Heat generation in electronics:

Heat generation in the electronics is simulated by usual bulk heat generation provided in ANSYS. The total heat generation in electronics is assumed to be 4.5 Watts, corresponding to 2.25 W per side. 87% of the heat is assumed to be generated in the 1st chips (l x w x h = 7.2 x 4.0 x 0.35 mm^3) and the rest is generated in the 2nd chip (l x w x h = 7.2 x 5.5 x 0.35 mm^3).

2.4 Heat generation in the silicon bulk:

The heat generation in the bulk of the radiation-damaged silicon detector is due to the bulk leakage current. The leakage current is known to have a strong temperature dependence:

$$I_{leak} \propto T^2 \cdot e^{-\frac{E_g}{2k_B T}} ,$$

where E_g is the effective gap energy of about 1.23 eV and k_B is the Boltzmann constant. In ANSYS program, the electrical resistance of material can be made temperature dependent. An electro-thermal element (SOLID67) is assigned for the bulk part of the silicon detector and it is assumed to carry an electrical conductance with the same temperature dependence as that of the leakage current [3].

Since the heat generation strongly depends on temperature, it must be standerized at specific temperature. It is proposed to use the heat generation per mm^2 of 300 μm thick silicon detector at 0˚C as a standard parameter. Actual heat generation is calculated using the T-dependence give above.

2.5 Comparison with experiments:

The thermal simulation were compared with various laboratory tests and agreement with test results are excellent, though convection as well as radiation from the surface of the test pieces had to be introduced with some adjustable parameters [3].

Thermal runaway was experimentally observed at KEK in a radiation damaged CDF-SVX microstrip detector [4]. A thermal simulation reproduced the observed runaway fairly well as shown in Figure 3.

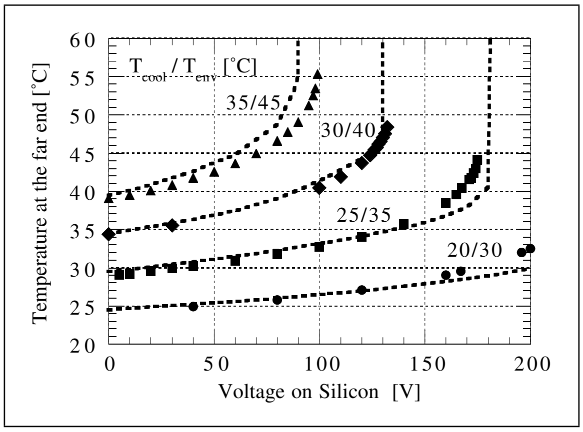

Figure 3 Thermal runaway observed in radiation damaged detector and thermal simulation[4]. T_{cool} and T_{env} are the temperatures of the cooling water and the vacuum vessel in which the runaway test is performed.

3. Results of thermal simulation

3.1 Typical thermal profiles

Figures 4 and 5 show typical thermal profiles of various views for the case of model TDR-1 with PG700, 4.5W in electronics power consumption, -10°C for the cooling temperature constraint, and 160 μW/mm² in bulk heat generation (at 0°C).

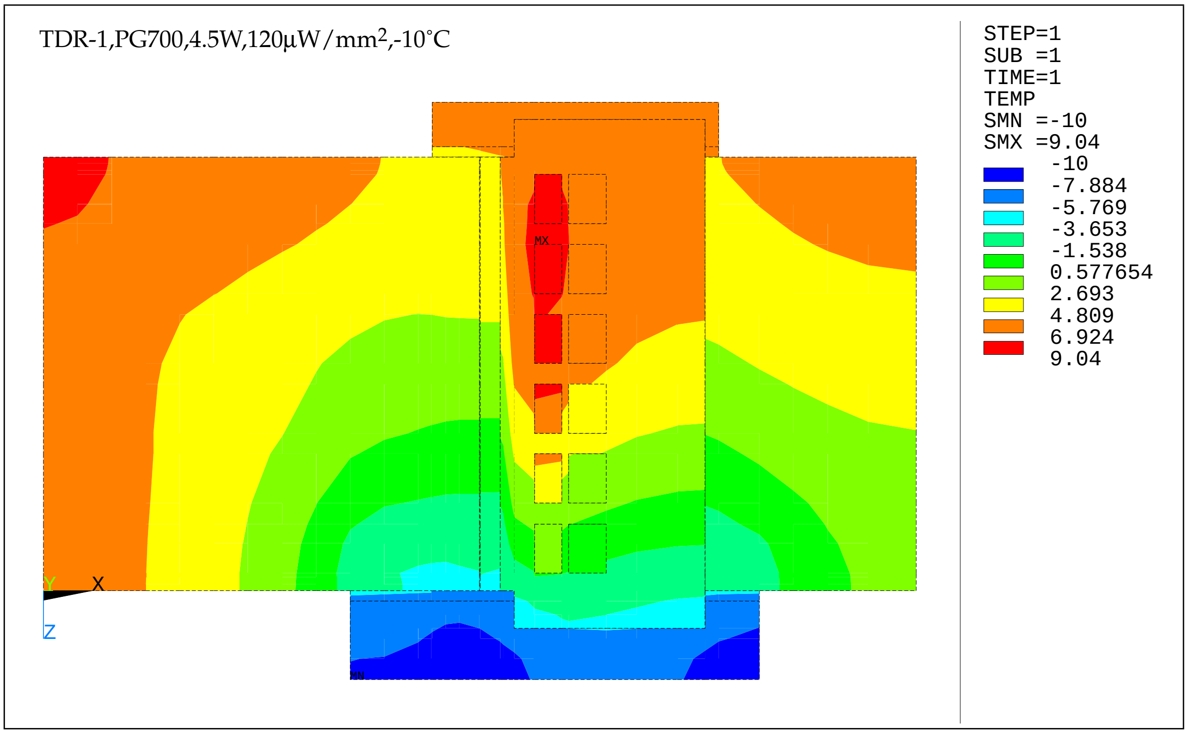

Figure 4 Top view of the thermal profile.

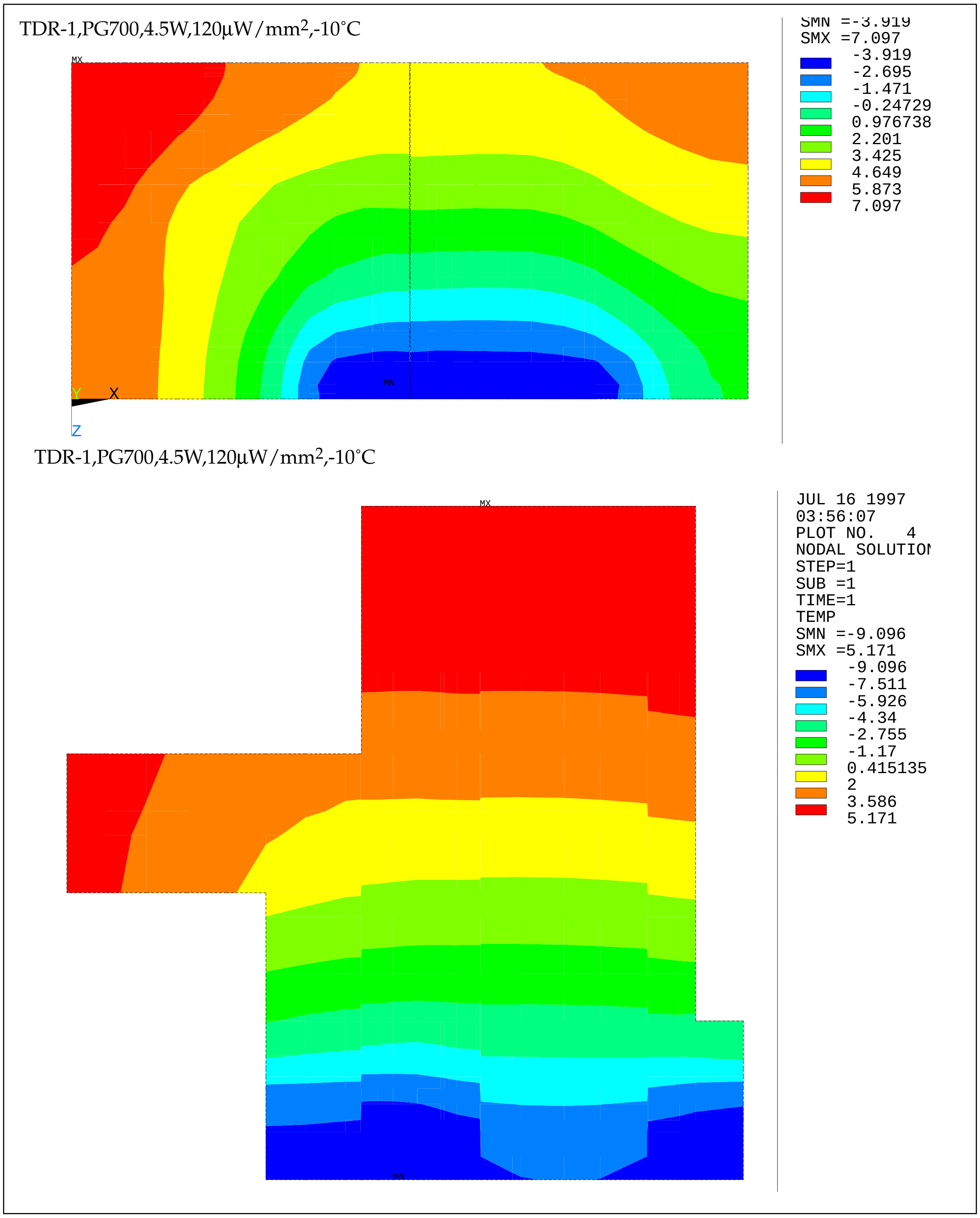

Figure 5 Thermal profile of the silicon detector (top view) and the baseboard (bottom view).

One sees that the case shown is close to the thermal runaway point, and therefore the maximum temperature in the silicon detector is seen at the top left corner as expected. In the profile of the baseboard, the apparent discontinuity in temperature is seen at the boundaries between PG and BeO plates where the gluing gaps exist.

3.2 Power in electronics

Figure 6 shows the dependence of the thermal behavior on the power consumption in the electronics, where Q_{amp} indicates the total summed power of all the electronics on the hybrids. The difference is quite large in the maximum temperature in the silicon detector, an order of 3°C. However the thermal runaway point is not so different. This is understandable because the runaway occurs at the corner of the silicon detector and thus it is independent of power consumption in electronics except thermal coupling near the cooling point.

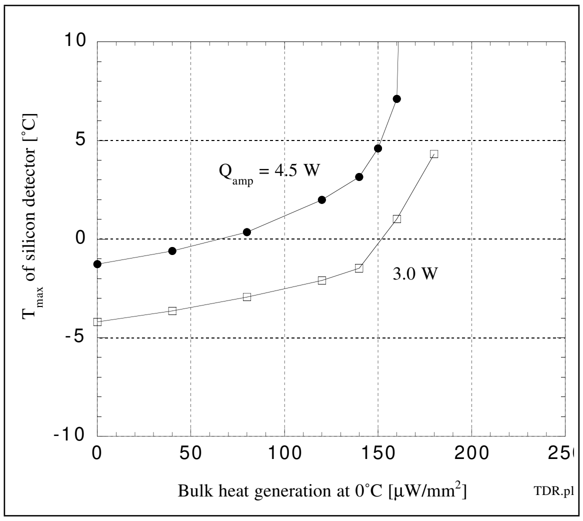

Figure 6 4.5W vs 3.0W in Qamp (TDR-1,PG700).

3.3 Thermal conductivity of PG

The thermal conductivity of PG is varied from 700 to 1700 in order to see the effectiveness of the PG. Figure 7 shows its dependence in model TDR-1. PG1700 shows the best performance as expected, but the improvement is rather small from PG1300. On the other hand, the difference between PG700 and PG1300 is substantial.

PG700 is used in the rest of simulation.

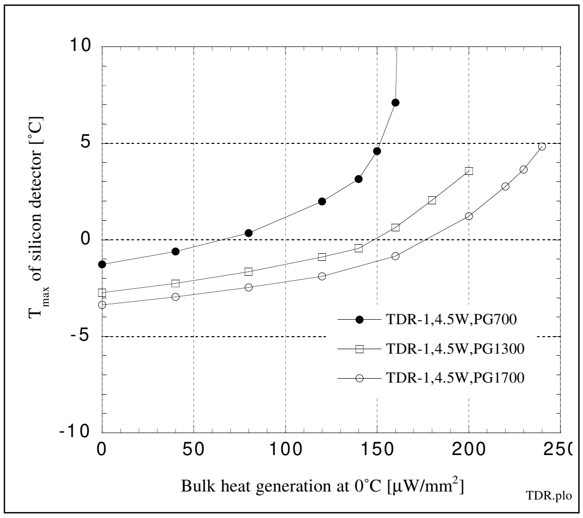

Figure 7 PG700 vs PG1300 vs PG1700.

3.4 PG versus BeO baseboards

Another way to see the effectiveness of PG is to replace the part or all of PG by BeO. As shown in Figure 8, all BeO (no PG) baseboard gives worse thermal behavior.

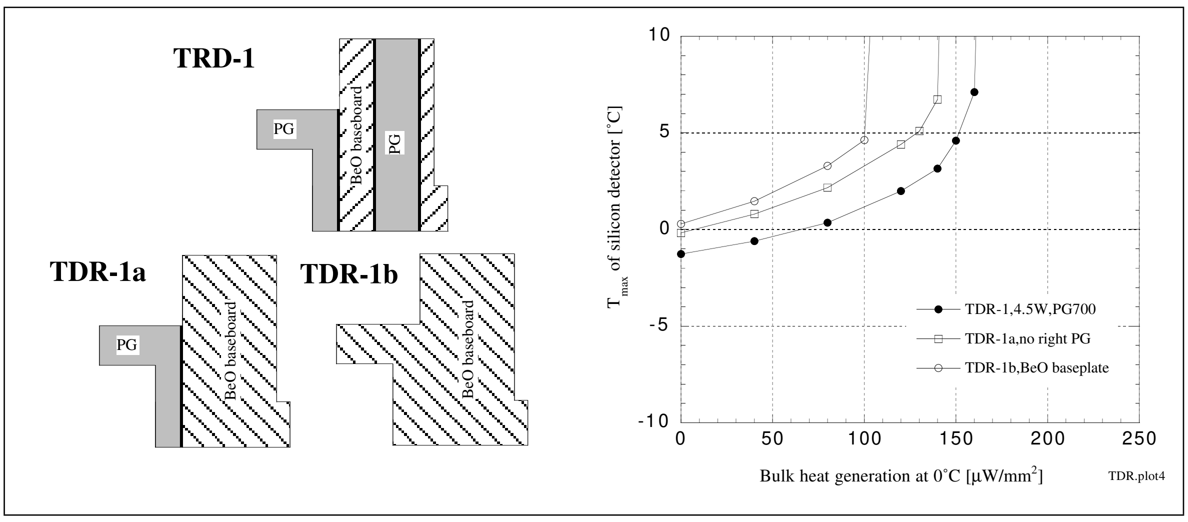

Figure 8 Baseboard dependence.

3.5 BeO cooling bar

The importance of the PG near the cooling side is demonstrated in Figure 9 in which model 1c has a BeO bar near the cooling channel instead of PG.

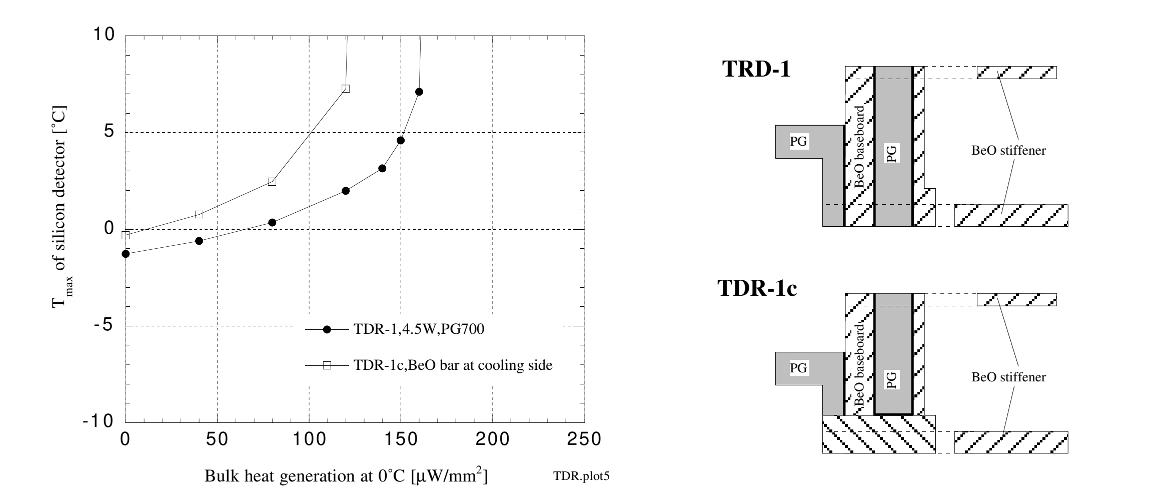

Figure 9 Baseboard dependence-2.

3.6 All PG baseboard

Although mechanically unstable, all the baseboard is assumed to be made of PG in model 1f. In addition, the BeO stiffeners near the cooling side is taken out in model 1g to see the thermal effect of the BeO stiffener. It seems the presence of stiffener makes little thermal effect.

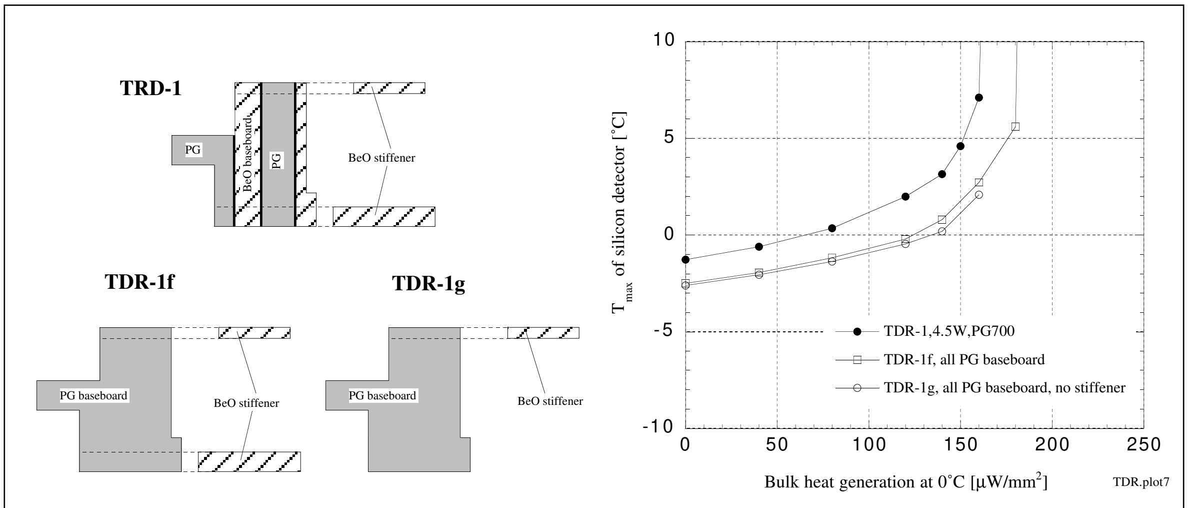

Figure 10 Baseboard dependence-3 and stiffener effect.

3.7 CFRP inserts

To strengthen the all-PG baseboard, four pieces of CFRP are added in the baseboard (model-1h). This model is similar to the one proposed by Univ. of Geneve group [5]. Figure 11 shows that the CFRP inserts give a little degradation but the effect is small. If an insulated stiffener is used on the far side of the cooling (model-1i), as proposed by the Geneve group, there is a small gain in performance but not much. Runaway point does not move from model-1h to -1i as expected.

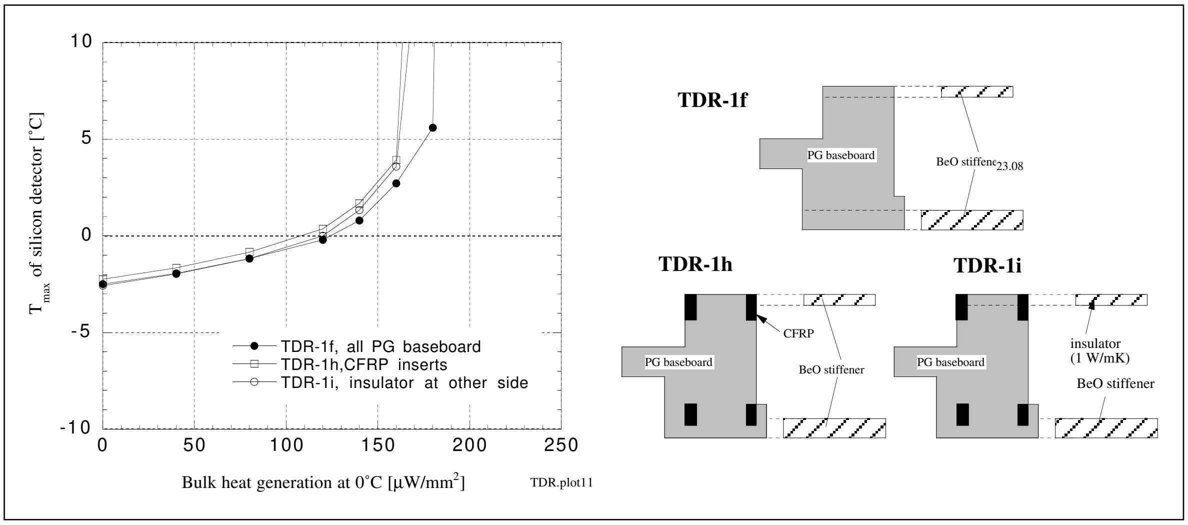

Figure 11 CFRP inserts and insulation for farther-side stiffener.

3.8 Length of the PG nose

The length of the PG nose is varied by +1 cm and -1 cm in Figure 12. The maximum temperature of silicon is identical up to 120 µW/mm^2. This is because the location of the maximum spot of silicon is near the BeO bridge below 120 µW/mm^2 . A small difference is observed after the maximum spot moves to the corner. The runaway point depends on the nose length, but the effect is small.

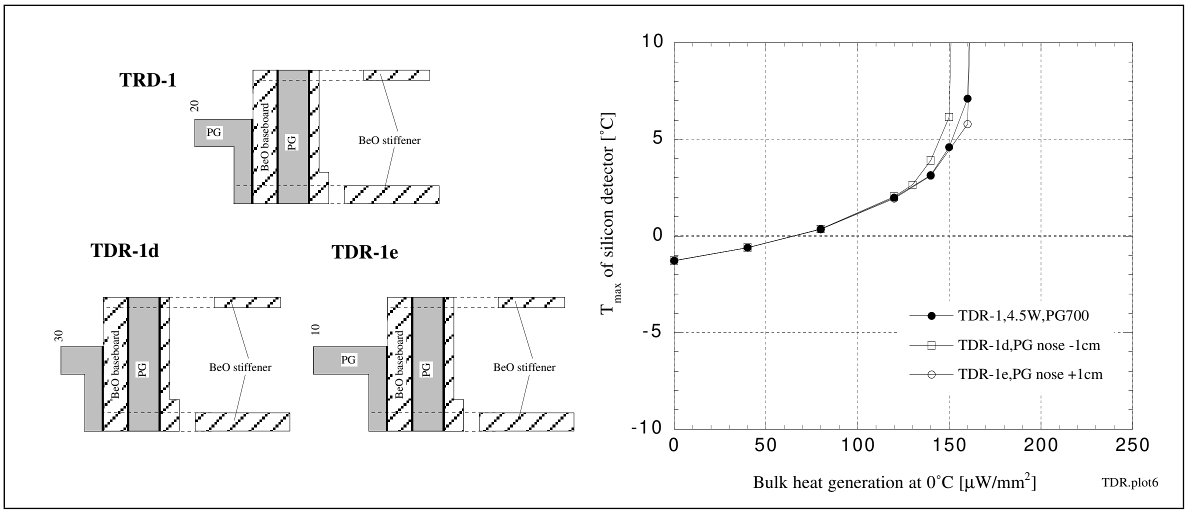

Figure 12 Length of the PG nose.

3.9 Model TDR-2

Model TDR-2 is introduced to eliminate the BeO stiffeners on both sides. However the PG part is replaced by BeO plates for structural support. Model 2a eliminates the middle BeO bypass while the PG nose is inclined in model 2b similar to one of the RAL proposals [6]. As shown in Figure 13, all models show worse thermal performance. This again indicates that the PG near the cooling point plays the most important role in the thermal properties of the module.

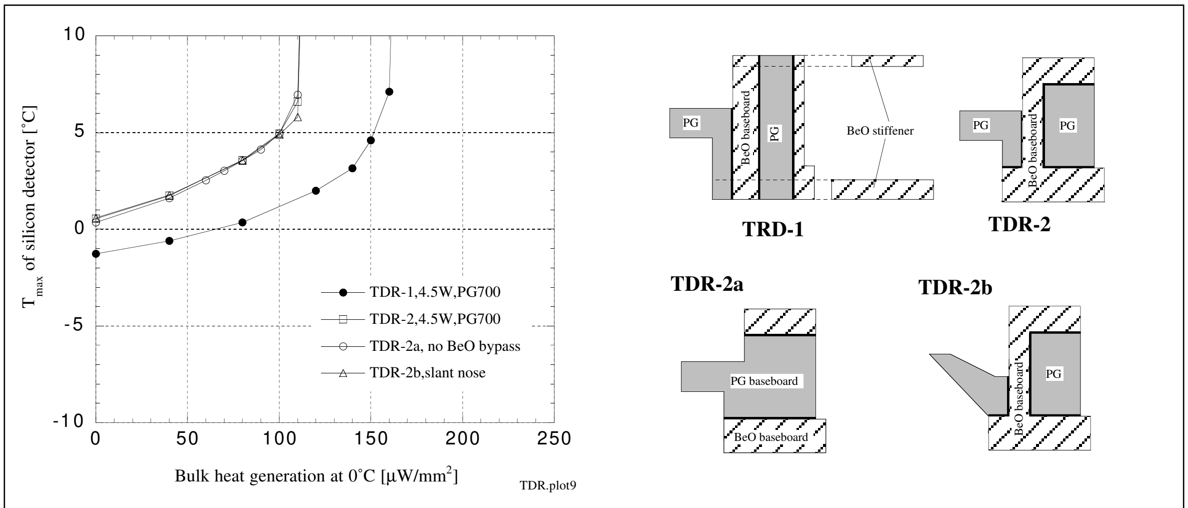

Figure 13 Model TDR-2 and its variation.

3.10 Dependence on T_{cool}

Figure 14 shows the dependence on the cooling temperature -15, -10 and -5 ˚C. The points with no bulk heat (0 μW/mm² @ 0˚C) are apart by 5 ˚C exactly. However, due to the non-linear T dependence of the leakage current, the higher the temperature, the faster the temperature rise. Accordingly the lowest cooling temperature is best for thermal point of view.

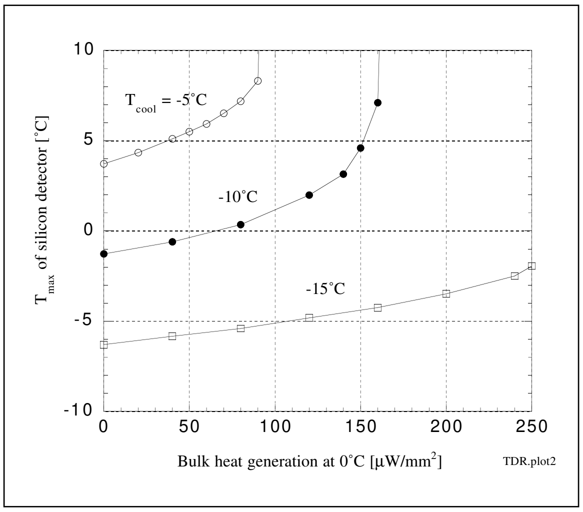

Figure 14 T_{cool} dependence.

3.11 Range of temperature

All the plots so far show the maximum temperature. Figure 15 shows both the difference ΔT_{Si} of the maximum and minimum of the silicon detector temperature with Q_{amp} = 3 and 4.5 W in model TDR-1. The ATLAS goal of $\Delta T < 3$˚C is difficult to be realized especiallywhen the power consumption in electronics is high. Model-1i with insuration on the farther side helps in reducing ΔT_{Si}.

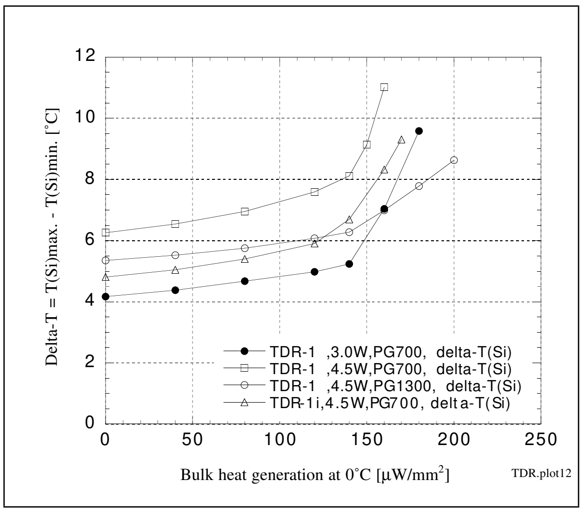

Figure 15 ΔT_{Si} = T(Si)max - T(Si)min.

4. Conclusions

The present thermal simulation based on the TDR model is summerized in the following:

1. The PG baseboard is needed. Replacing it by BeO degrades the thermal performance.
2. The PG part near the cooling channel plays the most essential role.
3. Power consumption of the electronics must be minimized to lower the average detector temperature, though the thermal runaway point is not so much affected.
4. PG1300 is much better than PG700 and the difference between PG1700 and 1300 is small.
5. All-PG baseboard shows superior thermal behavior.
6. The insuration on the farther side (from cooling) gives little difference.
7. No BeO stiffener models give less performance.
8. There are little dependence on the shape of the PG nose,
9. Lower cooling temperature is essential to get safety margin from thermal runaway.

References

[1] T. Kondo et al., Thermal simulation of ATLAS barrel SCT modules - I, May 27, 1997.

[2] ATLAS Inner Detector Technical Design Report, CERN/LHCC/97-17, 30 April 1997, Page 471.

[3] T. Kohriki et al., Cooling Test and Thermal Simulation of Silicon Microstrip Detectors for High Luminosity Operation, ATLAS Internal Note INDENT-NO-094.

[4] T. Kohriki et al., First Observation of Thermal Runaway in the Radiation Damaged Silicon Detector, IEEE Trans. Nucl. Sci. 43 (1996) 1200-1202

[5] G. Barbier et al., "TPG module", fax on 1.7.1997.

[6] RAL proposal A3-95, June 1997.